Fractional solubility of iron in mineral dust aerosols over coastal Namibia: a link with marine biogenic emissions?

Karine Desboeufs[1], Paola Formenti[1], Raquel Torres-Sánchez[2,3], Kerstin Schepanski[4,$], Jean-Pierre Chaboureau[5], Hendrik Andersen[6,7], Jan Cermak[6,7], Stefanie Feuerstein[4], Benoit Laurent[1], Danitza Klopper[8,*], Andreas Namwoonde[9], Mathieu Cazaunau[2], Servanne Chevaillier[2], Anaïs Feron[1,%], Cécile Mirande-Bret[1], Sylvain Triquet[1], and Stuart J. Piketh[8]

[1] Université Paris Cité and Université Paris Est Créteil, CNRS, LISA, F-75013 Paris, France

[2] Université Paris Est Créteil and Université Paris Cité, CNRS, LISA, F-94010 Créteil, France

[3] CIQSO, Robert H. Grubbs Building, University of Huelva, Campus El Carmen, E21071 Huelva, Spain

[4] TROPOS, Leipzig, Germany

[5] Laboratoire d'Aérologie (LAERO), Université de Toulouse, CNRS, UT3, IRD Toulouse, France

[6] Institute of Meteorology and Climate Research, Karlsruhe Institute of Technology (KIT), Karlsruhe, Germany

[7] Institute of Photogrammetry and Remote Sensing, Karlsruhe Institute of Technology (KIT), Karlsruhe, Germany

[8] North-West University, School for Geo- and Spatial Sciences, Potchefstroom, South Africa

[9] SANUMARC, University of Namibia, Henties Bay, Namibia

* Now at University of Limpopo, Department of Geography and Environmental Studies, Sovenga, South Africa

$ Now Institute of Meteorology, Freie Universität Berlin, Berlin, Germany

% Now at Université Paris-Saclay, INRAE, AgroParisTech, UMR ECOSYS, Palaiseau, France

Corresponding author: paola.formenti@lisa.ipsl.fr

Abstract

Mineral dust is the largest contributor to elemental iron in the atmosphere, and, by deposition, to the oceans, where elemental iron is the main growth limiting nutrient. Southern Africa is an important source at the regional scale and for the Southern Ocean, however limited knowledge is currently available about the fractional solubility of iron from those sources, as well as on the atmospheric processes conditioning its dissolution during deposition.

This paper presents the first investigation of the solubility of iron in mineral dust aerosols from 176 filter samples collected at the Henties Bay Aerosol Observatory (HBAO), in Namibia, from April to December 2017. During the study period, 10 intense dust events occurred. Elemental iron reached peak concentrations as high as 1.5 µg m^{-3}, significantly higher than background levels. These events are attributed to wind erosion of natural soils from the surrounding gravel plains of the Namib desert. The composition of the sampled dust is found to be overall similar to that of aerosols from northern Africa, but characterised by persistent and high concentrations of fluorine, which are attributed to fugitive dust from mining activities and soil labouring for construction.

The fractional solubility of Fe (%SFe) for both the identified dust episodes and background conditions ranged between 1.3 to 20 % and averaged at 7.9% (± 4.1%) and 6.8 (± 3.3%), respectively. Even in background conditions, the iron fractional solubility was correlated to that of aluminium and silicon. The solubility was lower between June and August, and increased from September onwards, during the austral spring months. The relation with measured concentrations of particulate MSA (methane sulfonic acid), solar irradiance and wind speed suggests a possible two-way interaction whereby marine biogenic emissions from the coastal Benguela upwelling to the atmosphere would increase the solubility of iron-bearing dust, according to the photo-reduction processes proposed by Johansen and Key (2006). The subsequent deposition of soluble iron could act to further enhance marine biogenic emissions. This first investigation points to the west coast of southern Africa as a complex and dynamic environment with multiple processes and active exchanges between the atmosphere and the Atlantic Ocean, requiring further research.

Keywords: aerosols, mineral dust, water-soluble Fe, atmospheric processing, marine biogenic emissions

1. Introduction

Through the processes of atmospheric transport and deposition, mineral dust is known to provide nutrients and metals to the terrestrial and marine ecosystems (Hooper et al., 2019; Ventura et al., 2021). Amongst those, mineral dust provides iron (Jickells et al., 2005), which plays a major role for the primary productivity of the nutrient-limited oceans, modulating the marine carbon cycle (Hooper et al., 2019) as well as that of key continental ecosystems such as the Amazon rainforest (Reichholf, 1986).

To date, much attention has been paid to the soluble Fe in mineral dust emitted from arid and semi-arid areas in the northern Hemisphere, in particular the Saharan and Chinese deserts (e.g. Baker et al., 2006; Paris et al., 2010; Takahashi et al., 2011; Rodriguez et al., 2021), where emissions are the most intense (Tegen and Schepanski, 2009). Nonetheless, the southern Hemisphere accounts for approximately 10% of the global atmospheric dust loading (Kok et al., 2017). Large sources are found in southern Africa, mostly in Namibia (Kalahari and Namib deserts, Etosha Pan, numerous ephemeral riverbeds along the Namibian coastline) and Botswana (Makgadikgadi Pan) (Prospero et al., 2002; Bryant et al., 2007; Mahowald et al., 2003; Ginoux et al., 2012; Vickery and Eckardt, 2013; Von Holdt et al., 2017).

Previous research has shown that the long-range transport of dust emitted from southern African sources can reach the south-eastern Atlantic and the Indian Oceans (Swap et al., 1996; Jickells et al., 2005; Bhattachan et al., 2012; 2015; Ito and Kok, 2017). In particular, Gili et al. (2022) demonstrated recently that mineral dust from Namibia can also be transported across the Southern Oceans to eastern Antarctica. Furthermore, the research by Dansie et al. (2022) has suggested that mineral dust from Namibia could dominate the atmospheric deposition to the coastal Benguela Upwelling System (BUS), where biomass burning aerosols, a significant source of soluble Fe to the Southern and Indian Oceans (Hamilton et al., 2021; Ito et al., 2021; Liu, et al., 2022), are limited by atmospheric stratification (Formenti et al., 2019; Redemann et al., 2021). The inputs of Namibian (and Angola) dust in the upwelled waters could also modulate the migration of skipjack tuna between Gulf of Guinea and equatorial Atlantic, by contributing to support phytoplankton growth and hence upper trophic levels in this area (Rodriguez et al., 2023).

There is, however, very little data available on the concentrations and composition of soluble Fe in dust aerosols from southern Africa, both near the sources and over the oceans. Previous research in Namibia focussed on soils and sediments (Dansie et al., 2017a; 2017b; Kangueehi, 2021). The Atlantic Meridional Transect (AMT) cruise programme conducted recurrent observations between October and March in the South Atlantic Ocean (Baker et al., 2013), while Heimburger et al. (2013) and Gao et al. (2013) report on sparse measurements of deposited aerosols and in rainwaters over the Southern Indian Ocean.

Within this context, this paper investigates the fractional solubility of Fe in samples of atmospheric aerosol particles smaller than 10 µm in diameter collected in 2017 at the Henties Bay Aerosols Observatory (HBAO; 22.09°S, 14.26°E) on the Namibian coast. In section 2 we outline the experimental and analytical methodology for elemental and water-soluble analysis of ions and metals, including iron. We also provide the definition of fractional solubility and method for estimating the total dust mass. We introduce the supporting tools used to evaluate the source regions of the collected mineral dust, their pathways during transport, and the presence of fog, a recurrent feature on coastal Namibia favouring multi-phase ageing processes. Section 3 provides the results of the analysis. We present the iron soluble concentrations and solubility, and explore their links to the load, emission area and transport of mineral dust, as well as atmospheric processing. Section 4 discusses the observations, suggesting that the fractional solubility of iron in the Namibian dust is higher when the MSA, a tracer of marine biogenic emissions, is also detected in highest concentrations. This points to the photo-oxidation of DMS as a process for increasing the Fe solubility, and suggests a possible positive feedback loop of the iron fertilisation by dust to the ocean. Section 5 summarizes the findings and suggests directions for future research.

2. Methodology

2.1. Study area

The Henties Bay Aerosol Observatory (HBAO, 22.09°S, 14.26°E; http://www.hbao.cnrs.fr/, last access: 10 October 2022) is located at the Sam Nujoma Marine and Coastal Resources Research Centre (SANUMARC) of the University of Namibia in Henties Bay, Namibia (**Fig 1**).

Fig 1. *Location of Henties Bay Aerosol Observatory (HBAO, red star) and main dust source regions (© Google Maps). The position of Walvis Bay (blue dot), the major harbour in the area, and the Wlotzkasbaken meteorological station (blue star) are also indicated.*

Three kilometers to the south of the University campus hosting HBAO is the small town of Henties Bay, with no industrial activity and very little traffic, and approximately 170 km north from Walvis Bay, the major harbour in Namibia. Directly east of HBAO are the Namibian gravel plains, which are one of the dominant features of the Namib desert together with the sand dunes. Approximately 100 m to the north is the Omaruru riverbed, one of the coastal sources of mineral dust identified by Vickery and Eckardt (2013).

Our previous results show that, at the surface level, the atmosphere at HBAO is a receptor of different air masses dominated by marine aerosols, but also the seasonal occurrence of light-absorbing aerosols from biomass burning or pollution in northern wind regimes, and mineral dust detected episodically from various wind directions (Formenti et al., 2018; Klopper et al., 2020, hereafter KL20).

2.2. Sample collection and analysis

Aerosol particles smaller than 10 μm in aerodynamic diameter (PM_{10}) were collected by an automated sampler (model Partisol Plus 2025i, Thermo Fisher Scientific, Waltham, MA USA) on 47 mm Whatman Nuclepore polycarbonate filters (1-μm pore size). The air was drawn through a certified sampling inlet (Rupprecht and Patashnick, Albany, New York, USA) located at approximately 30 m above ground and operated at a flow rate of 1 m^3 h^{-1}. Samples were collected for 9 hours during the daytime (from 9:00 to 18:00 UTC time) and night-time (21:00 to 06:00 UTC time) for 12 non-consecutive weeks

5

from April to December 2017 (7-14 April, 26 April-3 May, 19-26 May, 07-14 July, 2-9 August, 15-22 August, 18-25 September, 02-09 October, 31 October-7 November, 13-20 November, 28 November-04 December, 12-19 December). In total, 176 samples (+ 13 blanks, one per week of sampling) were collected.

The elemental analysis of 24 elements from Na to Pb and including some major tracers of mineral dust (Fe, Al and Si) was performed at the LISA laboratory by Wavelength-dispersive X-ray fluorescence (WD-XRF) using a PW-2404 spectrometer (Panalytical, Almelo, Netherlands), as detailed by KL20. The total mass concentration per element x will be referred to as TX.

The measured elemental concentrations are used to calculate the estimated dust mass (*EDM*) according to Lide (1992) as

$$EDM = 1.12 \times \{1.658 \times [nss\text{-}Mg] + 1.889 \times [Al] + 2.139 \times [Si] + 1.399 \times [nss\text{-}Ca] + 1.668 \times [Ti] + 1.582 \times [Mn] + (0.5 \times 1.286 + 0.5 \times 1.429 + 0.47 \times 1.204) \times [Fe]\} \qquad (1)$$

where, as explained by KL20, nss-Mg and nss-Ca represent the non-sea salt fractions of Mg and Ca, respectively.

The analysis of the water-soluble fraction was also performed at LISA. Individual filters were placed in 20 mL of ultrapure water (MilliQ® *18.2* MΩ.cm) for 30 minutes. The solution was filtered (Nuclepore polycarbonate filters with 0.2μm pore size) then divided into two sub-samples. One half was analysed by Ion Chromatography (IC) using a Metrohm IC 850 device equipped with a column MetrosepA supp 7 (250/4.0 mm) for anions and with a Metrosep C4 (250/4.0 mm) for cations. The IC analysis provided the concentrations of the following water-soluble ions: F^-, Cl^-, NO_3^-, SO_4^{2-}, formate, acetate, oxalate, MSA^- (methanesulfonic acid), Na^+, NH_4^+, K^+, Ca^{2+} and Mg^{2+}. A calibration with certified standard multi-ions solutions of concentrations ranging from 5 to 5000 ppb was performed and the uncertainty of the analysis was estimated to be 5% (KL20).

The second half of the solution was acidified to 1% with ultrapure nitric acid (HNO_3) and analysed by Inductively Coupled Plasma-Atomic Emission Spectroscopy (ICP-AES) using a Spectro ARCOS Ametek® ICP-AES and by High-resolution Inductively Coupled Plasma-Mass Spectrometry (HR-ICP-MS) using a Neptune Plus™ instrument by Thermo Scientific™. The calibration curve was performed using standard multi-element solutions ranging from 2 to 1000 ppb for ICP-AES and 1 to 1000 ppt for HR-ICP-MS (Desboeufs et al., 2022). These analyses provided the dissolved mass concentrations (DX) of 25 water-soluble metals and metalloids, including Fe, Al, and Si. All sample concentrations were corrected using the filter blanks for each sampling period.

Based on those analyses, the fractional solubility (%SX) representing the percentage solubility value was calculated as

170

$$\%SX = 100 \times DX/TX \qquad (2)$$

172

with DX and TX, the dissolved and total elemental concentration respectively.

Here, a leaching protocol using ultrapure water (UPW) was used to simulate wet deposition of parti-cles, since the wet deposition dominates the total iron supply in the Southern Atlantic Ocean (Chance et al., 2015). Moreover, the UPW leach enables the chemical reaction between iron with organic or inorganic ligands, naturally dissolved from the particulate aerosols into rain droplets. However, it is known that the extraction protocol modulates dissolution process and hence the values of iron frac-tional solubility, in particular the estimates using UPW are higher in comparison to these one using seawater, but lower than the acidic, buffered or reduction agent leach (Perron et al., 2020).

2.3. Ancillary data

Maps of the emission fluxes of mineral dust were calculated using the dust emission model described by Feuerstein and Schepanski (2019), driven with hourly 10m wind fields at a 0.1° x 0.1° grid from the European Centre for Medium-range Weather Forecasts (ECMWF). The dust emission parame-terisation follows Marticorena and Bergametti (1995). Additional information on the soil type was taken from the ISRC soil data set (FAO/IIASA/ISRIC/ISSCAS/JRC, 2012) and information on the aerody-namic roughness length was obtained from POLDER/ADEOS surface products following the works of Marticorena et al. (2004) and Laurent et al. (2005). The MODIS monthly vegetation product (MYD13A3 v6) was used to describe the vegetation cover, while the vegetation type was defined using the BIOME4 database (Kaplan et al., 2003). We additionally differentiated between different dust source types (alluvial fines, dunes and sand sheets) which allowed us to reflect the source di-versity over Namibia and thus the spatial diversity in the soil's susceptibility to wind erosion. This layer was compiled following Feuerstein and Schepanski (2019) using MODIS surface reflectance (MOD09A1 v6). A MODIS retrieved map on surface water cover was used to eliminate flooded areas as active dust sources.

Back-trajectories of the air masses during the dust event were calculated from Meso-NH model (ver-sion 5.3). The model set-up is similar to the one used for the AErosols, RadiatiOn and CLOuds in southern Africa (AEROCLO-sA) field campaign (Formenti et al. 2019) and related case studies (Fla-mant et al. 2022; Chaboureau et al. 2022). In short, the model was run on a 5 km grid covering the southern tip of Africa and 67 stretched levels spaced by 60 m close to the surface and 600 m at high altitude. Meso-NH was run for 24 h for each dust event using initial and boundary conditions provided by the ECMWF operational analysis. Emission, transport and deposition of dust is described by the scheme of Grini et al. (2006). Back trajectories were computed online using three passive tracers

204 initialized with the 3D-field of their initial conditions. Further details on the dust prognostic scheme,
205 the backward trajectories and the physical parameterizations are given in Chaboureau et al. (2022).

206 The presence of fog and low clouds (FLC) along the Namibian coastline during dust events was an-
207 alysed using an existing satellite-based fog and low-cloud data set (Andersen et al., 2019). The FLC
208 detection algorithm used to create this data set was developed and validated specifically for this re-
209 gion. The algorithm is based on infrared observations from the Spinning Enhanced Visible and Infra-
210 red Imager (SEVIRI) aboard the geostationary Meteosat Second Generation (MSG) satellites, making
211 use of both spectral and textural information. The FLC product is available at the native spatial and
212 temporal resolutions of the SEVIRI sensor (3 km nadir, every 15 minutes), as described in Andersen
213 and Cermak (2018). The FLC product does not specifically distinguish between fog and low clouds
214 but captures the coastal boundary-layer cloud regime typical for the region and at HBAO that could
215 interact with mineral dust. It has been shown to be consistent with synoptic-scale atmospheric dy-
216 namics (Andersen et al. 2020). The FLC data are used to calculate maps of average fog and low
217 cloud coverage for the time periods of all dust events given in Table 1.

218 Observations of the local meteorology, including measurements of air temperature, relative humidity
219 and fog, at the nearby Wlotzkasbaken meteorological station (22.31°S, 14.45°E, 73 m asl, see **Fig.**
220 **1**) part of the Southern African Science Service Centre for Climate Change and Adaptive Land Man-
221 agement (SASSCAL) ObservationNet (https://www.sasscal.org/; last accessed 14/04/2023), are
222 used.

223

224 **3. Results**

225 **3.1.   Description of the dust episodes**

226 The dataset discussed in this paper is based on 176 aerosol samples collected at HBAO, 42 of which
227 were associated with 10 dust episodes. As detailed by KL20, events of mineral dust were identified
228 as peaks in the time series of the mass concentrations of Al and non-sea-salt Ca^{2+} (nss-Ca^{2+}). The
229 dust episodes investigated in this study are a subset of those presented by KL20, we therefore use
230 their naming convention to facilitate the connections between the two papers (**Table 1**). In the follow-
231 ing, we refer to samples collected during the dust episodes as "dust". Samples collected outside the
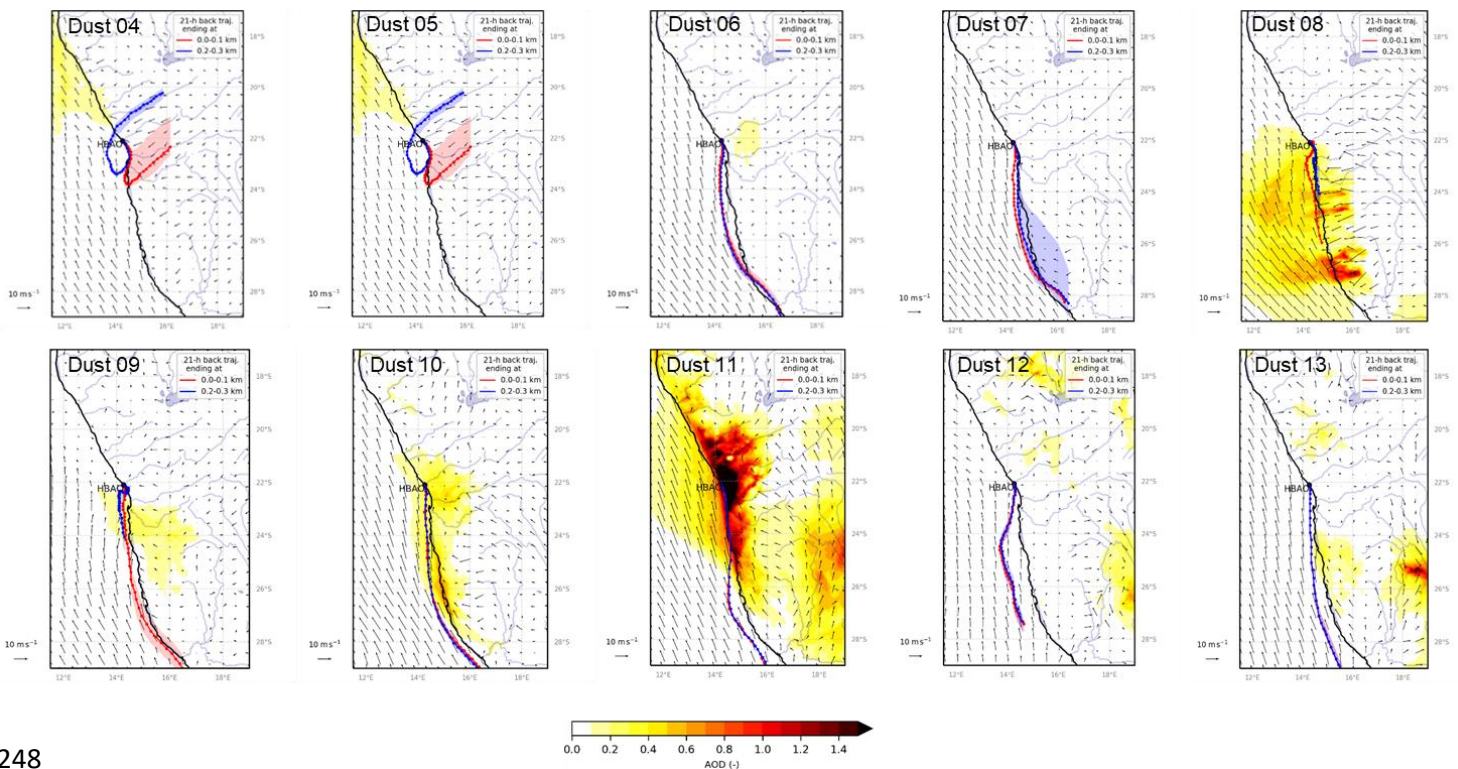232 dust events will be indicated as "background".

233
234 **Table 1.** *Dates of dust events identified at HBAO from May to December 2017, following KL20. The number of*
235 *samples collected during each episode is indicated in the column called "N". The average air temperature,*
236 *relative humidity, wind speed and direction recorded at the nearby meteorological station in Wlotzkasbaken are*
237 *reported. The maxima wind speed and corresponding direction are indicated in brackets in the corresponding*
238 *columns. The average EDM is reported with in brackets the maximum of EDM during the event.*

Episode identifier	Start and end date (UTC)	N	Air tempera-ture (°C)	RH (%)	Wind speed	Wind direc-tion (degN)	EDM

					(m s^{-1})		(µg m^{-3})
Dust 04	19/05 09h – 20/05 18h	3	17.7	73.7	2.7 (6.2)	186 (185)	13 (14)
Dust 05	24/05 21h – 26/05 09h	3	18.1	63.3	2.3 (6.3)	183 (188)	21 (42)
Dust 06	11/07 09h – 13/07 09h	4	13.2	82.9	1.2 (5.4)	235 (193)	27 (45)
Dust 07	04/08 21h – 06/08 09h	4	12.5	87.0	1.2 (5.4)	233 (201)	10 (16)
Dust 08	17/08 21h – 19/08 09 h	4	11.9	80.6	1.3 (4.6)	324(129)	18 (21)
Dust 09	23/09 21h – 24/09 18h	2	15.6	84.3	3.1 (6.2)	309 (330)	11 (17)
Dust 10	05/10 21h – 08/10 09h	8	14.0	74.6	2.1 (5.9)	249 (228)	14 (23)
Dust 11	15/11 09h – 18/11 09h	6	16.7	66.1	3.2 (11.7)	231 (232)	31 (56)
Dust 12	30/11 09h – 01/12 18h	3	16.7	78.1	1.9 (5.7)	244 (195)	2 (3)
Dust 13	15/12 09h – 19/12 09h	7	16.9	76.9	2.9 (6.5)	252 (238)	10 (19)

239

The dust episodes were long-lasting (generally a few days). The dynamic of the emissive areas, air mass transport and fog coverage during the episodes (**Fig. 2 and S1**) is driven by the synoptic circulation, which, in southern Africa, is primarily affected by the high-pressure belt under the descending limb of the Hadley cell (Tyson and Preston-Whyte, 2014). The maps of dust emission fluxes and the air mass back-trajectories reflect this seasonality. During the first part of the year (episodes Dust 04 to 05), dust emissions originated from the gravel plains and the Etosha pan north of HBAO. During this time of the year the transport to HBAO below 300 m asl was north- to south-easterly originating inland from the coast.

248

9

Fig 2. *Maps of dust optical depth (shading) and 10-m wind (vector) overlaid by pathway of 21-hour air mass back trajectories ending in the first 100 m (red line) and between 200 and 300 m (blue line) above HBAO for dust episodes, as calculated by the Meso-NH model (version 5.3). Dots are plotted every hour and shadings around these lines are the interquartile ranges for latitudes.*

From July onwards, the active source areas were identified in the southern gravel plains, Namib sand dunes and Kalahari Desert (this former only for Dust 11 to 13). Air mass transport was southerly and travelled over the sea and along the coastline. It is worth noticing that all the air masses experienced maritime air during their last hours of transport, including the episodes Dust 04 and 05 associated with berg wind conditions, due to the coastal low that develops to the west of HBAO.

The formation of fog events at Henties Bay is also highly seasonal. The frequency of occurrence of fog events is highest during austral winter at the coast, whereas lifted stratus clouds dominate during austral summer, when overall FLC occurrence peaks. The occurrence of fog over Namibia correspond to the advection of low-level clouds which is modulated both by local meteorology along the coastline of Namibia (trade winds) and synoptic-scale radiative processes (Spirig et al., 2019; Andersen et al., 2019; 2020). Henceforth, as shown in Fig. S1, the presence of fog and low clouds correlates with wind directions and aerosol source regions. Overall, three episodes (Dust 04, Dust 05 and Dust 11 in April, May and November, respectively) occurred in fog-free or low-fog conditions. The remaining episodes were characterised by extensive fog and low cloud coverage throughout the study area. The meteorological observations at the nearby Wlotzkasbaken station (**Fig. S2**) confirm these findings, and show in particular that the relative humidity always exceeded 60 %, and 80 % when fog or low clouds were present (Table 1). As a consequence, the aerosol can be considered deliquescent even in the fog-free conditions. The seasonality is also observed in the average downwelling solar irradiance, with the lowest values during July and September, associated with austral winter. Finally, it is interesting to note that the fog-free conditions, associated with the predominance of continental air masses, corresponded to the highest estimated dust mass (EDM), possibly because of the reduced wet removal during transport and the increase of emission fluxes with the decrease of soil moisture (Kok et al., 2014), but possibly also because of the high wind speed prevailing during these conditions, which in principle, enhances both dust emissions and transport (Table 1).

3.2. Iron solubility

The total and dissolved concentrations, and fractional solubility of Fe, Al and Si, during the dust episodes are reported in **Table 2,** where they are compared to background conditions. For iron, the average values over the entire sampling period are also shown.

Table 2. *Average and standard deviations of water-soluble (DX), total elemental (TX) mass concentrations and fractional solubility (%SX) for Fe, Al and Si at HBAO measured for the total period and during the dust and background events from April to December 2017. Concentrations values are expressed in ng m^{-3}, while fractional solubility is expressed in percent. The numbers of considered samples is presented between the parentheses.*
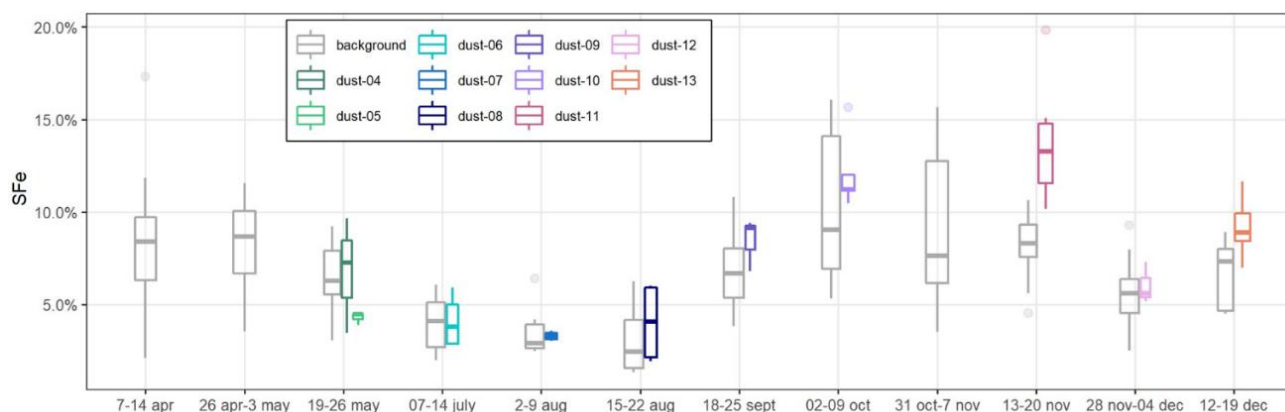
	Fe			Al		Si	
	All period	**Dust**	**Background**	**Dust**	**Background**	**Dust**	**Background**
DX	28 ± 51 *(N=175)*	80 ± 84 *(N=42)*	11 ± 10 *(N=131)*	322 ± 296 *(N=42)*	56 ± 46 *(N=131)*	529 ± 616 *(N=42)*	78 ± 83 *(N=124)*
TX	364 ± 482 *(N=176)*	955 ± 633 *(N=42)*	177 ± 155 *(N=133)*	1204 ± 870 *(N=42)*	284 ± 222 *(N=94)*	4158 ± 3037 *(N=42)*	776 ± 674 *(N=133)*
%SX	7.1 ± 3.6 *(N=175)*	7.9 ± 4.1 *(N=42)*	6.8 ± 3.3 *(N=130)*	27 ± 10 *(N=42)*	26 ± 11 *(N=90)*	12 ± 7 *(N=42)*	11 ± 8 *(N=116)*

The total Fe concentrations varied significantly from one episode to the other, and so did EDM, which was larger than 10 µg m^{-3} for all of them (except Dust 12) and as high as 56 µg m^{-3} during Dust 11 event (Table 1). By contrast, the total Fe-to-EDM ratio was virtually constant, with an average of 5.8 % (± 0.6 %) for the dust events and 5.6 % (± 1.1%) for the entire dataset. These values are quite superior to usual Fe content recommended in upper continental crust models (3.5% for Taylor and McLennan or 5.04 +/- 0.53 % Rudnick and gao, 2004) and estimated in Saharan dust (4.45% for Guieu et al., 2002; 4.3 to 6.1% for Lafon et al., 2006 or 4.5% for Formenti et al., 2008). Keeping in mind that Fe abundance is estimated, this suggests that the Namibian aerosol dust could be enriched in iron in comparison to upper crust and dust provided by Saharan sources.

The total dissolved concentrations of Fe during the sampling period ranged from 1.5 to 427 ng m^{-3}, with a median and average of 10.5 and 28 ng m^{-3}. During the dust episodes, the average mass concentration of dissolved Fe was 80 ± 84 ng m^{-3}, almost an order of magnitude higher than for background conditions (11 ± 10 ng m^{-3}). The dissolved concentrations in dust periods are higher than those observed in the South Atlantic Ocean for air masses associated with transport from continental southern Africa (Baker et al., 2013; Chance et al., 2015; Baker and Jickells, 2017), which are of the order as those observed at HBAO for background periods. The calculated fractional solubility of Fe ranged from 1.3 to 19.8 %, with a median and average of 6.7 and 7.1 %. The average %SFe during dust events (7.9 ± 4.1%) was higher, but quite similar than in background conditions (6.8 ± 3.3%). It is interesting to note that Dust 11 event, the most intense recorded event, presents the highest %SFe (between 10.2 and 19.8 % with an average at 13.8 %). Apart from this event, the average fractional solubility seems to be independent of the EDM. Excluding this event, the average solubility of Fe for dust event (6.9 % ± 3.3 %) is equivalent to the one for background samples. The uniformity of iron solubility values between background and dust periods contrasted with the observations made in regions where the dust influence is sporadic and the origin of Fe is associated to various sources (e.g. Shelley et al., 2018). That is consistent with a main dust source of iron in our samples, as indicated in KL20. For both conditions, the observed range of variability is high and consistent with previous observations over the Southern Atlantic Ocean (2.4-20 %, Baker et al., 2013; 1.3-22 %, Chance et al., 2015), and the Southern Indian Ocean (0.76-27 %, Gao et al., 2013), using acetate buffer leach
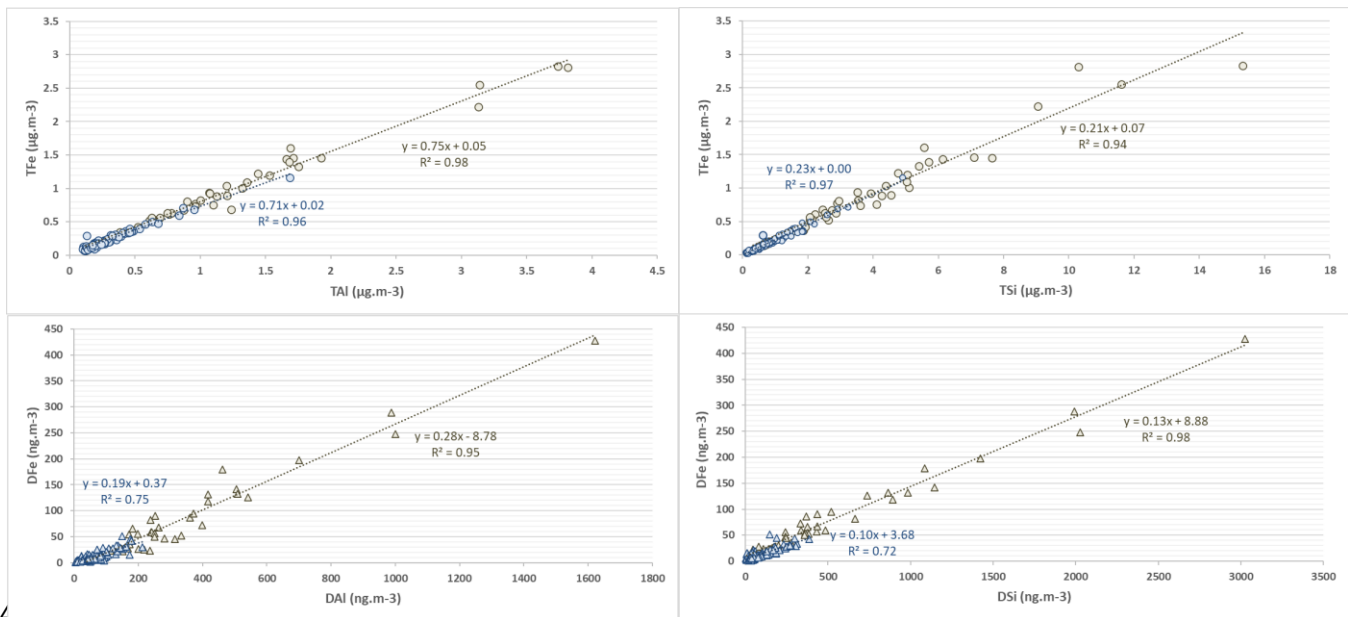
at pH 4.7 (0.4μm) which can extract 1.4 times more Fe than UPW protocol (Perron et al., 2020). Moreover, the measured iron fractional solubility is significantly higher than obtained from dissolution experiments, with an identical protocol, of mineral dust aerosol samples collected on filters after laboratory generation from the soils collected in Namibian sources (< 1%; Formenti et al., in preparation, 2024).

Fig.3: *Temporal variability of %SFe average for dust and background samples during the different periods of sampling. In the box plots, the box indicates the interquartile range, i.e. the 25th and the 75th percentile, and the line within the box marks the median. The whiskers indicate the quartiles ±1.5 times the interquartile range. Points above and below the whiskers indicate outliers outside the 10th and 90th percentile.*

The temporal variability of %SFe is presented in **Fig. 3**, where dust and background episodes are shown separately. The temporal variability is similar during dust and background conditions. The highest %SFe occurred during austral spring (October-November), and in particular during episode Dust 11 from 13 to 20 November 2017, when the average %SFe reached 13.8 %. The %SFe was quite similar along the year between dust and background, except between 13-20 November where the iron solubilities during Dust 11 event was very superior to the one of background samples, and to a lesser extent, in September (Dust 09) and December (Dust 13).

Fig. 4. *Scatterplot of TFe with respect to TAl and TSi (top panels) and DFe with respect to DAl and DSi (bottom panels) for dust (sand dots and triangles) and background events (blue dots and triangles). The Pearson coefficient are shown for both.*

Fig. 4 represents the correlations of Fe with Al and Si, both for the total and the dissolved concentrations. For both dust and background samples, the total Fe concentration is linearly correlated with total Al (R^2=0.98 and 0.96, slope=0.75 and 0.71, for dust and background conditions respectively) and total Si (R^2=0.94 and 0.97, slope=0.21 and 0.23, respectively). The slopes are consistent with typical Fe/Al and Fe/Si ratios found in desert dust from northern Africa (Formenti et al., 2011; Shelley et al., 2014), confirming the main crustal origin of Fe during all the sampling periods. Likewise, the concentrations of dissolved iron (DFe) show a strong linear correlation with both DAl and DSi, for both for dust and background events (R^2=0.96 and 0.75 with respect to DAl and R^2=0.98 and 0.73 with respect to DSi). The slopes for Al and Si are also comparable (0.19 and 0.28 for DAl and 0.10 and 0.13 for DSi, respectively in dust and in background events). A very strong linear correlation was also observed between DFe and DTi (R^2=0.96 and 0.84; not shown), another unique marker of mineral dust. Significant correlations of soluble concentrations for several elements associated with mineral dust (Fe, Al, Si, Ti) have been previously obtained in remote aerosols over ocean area (Baker et al., 2016). Additionally, DFe during dust events correlate very closely with F$^-$ (R^2=0.94, not shown), which has been indicated by KL20 as being emitted in the atmosphere by the wind erosion as well as the labouring of the Namibia soil, rich in fluoride mineral deposits.

4.   Discussion

Several studies have showed that variations in aerosol Fe solubility could result from the source/composition of the aerosols. As a matter of fact, the Fe solubility has been linked to the iron mineralogy
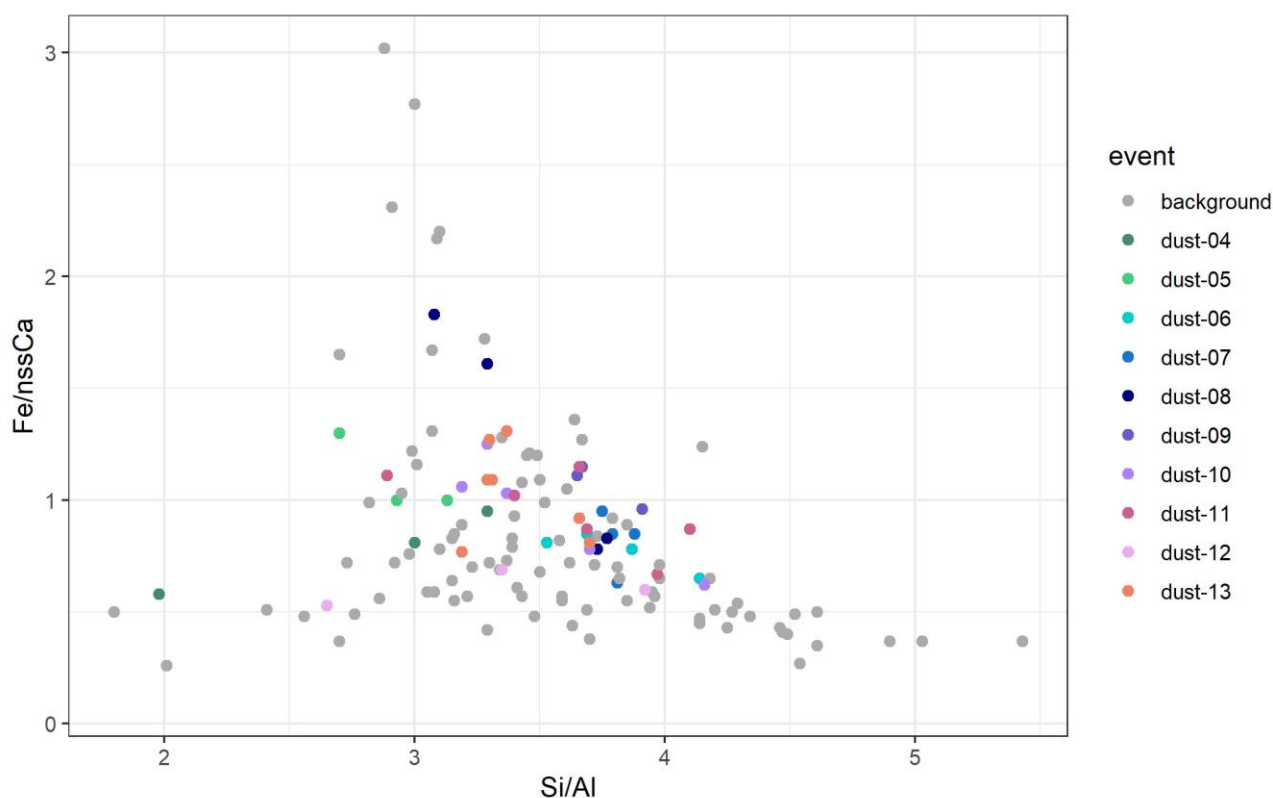
359 (Journet et al., 2008) and has been shown being lower for African crustal sources than in continen-
360 tal/anthropogenic sources (Desboeufs et al., 2005; Sholkovitz et al., 2009; Shelley et al., 2018). The
361 iron fractional solubility in mineral dust is also affected by source mixing (Paris et al., 2010; Desboeufs
362 et al., 2005), by (photo)chemical processing with acids or organic ligands during atmospheric
363 transport (Paris et al., 2011, Paris et Desboeufs, 2013; Wozniak et al., 2013; Swan and Ivey, 2021)
364 and by the increase of surface area to volume ratio due to size changes during transport (Baker &
365 Jickells, 2006; Marcotte et al., 2020).

366 In the following sections, we discuss these possible factors to explain the seasonality and the ex-
367 tended range of variability of the fraction Fe solubility in HBAO samples. The possible increase of
368 surface area to volume ratio during transport (Baker and Jickells, 2006; Marcotte et al., 2020) will not
369 be discussed because of lack of appropriate observations of the size distribution. Because of the
370 similar transport time suggested by back trajectories (Fig.2), it is likely that particle size distribution
371 would be similar from one event to the other.

372 **4.1. Influence of dust composition**

373 Close to dust source, iron solubility could be mainly conditioned by the mineralogical composition of
374 dust (Journet et al., 2008, Formenti et al., 2014). Considering that soluble Fe-bearing aerosols were
375 issued from mineral dust for all the samples, the seasonality of dust emission sources (see 3.1) could
376 be a factor explaining the seasonality of %SFe (and other elements associated to mineral dust). **Fig.**
377 **5** shows the scatter plot of the elemental mass ratio of $Fe/nss-Ca^{2+}$ and Si/Al, previously used for
378 northern Africa dust to distinguish aerosol dust from source areas enriched in clays or iron oxides to
379 soils rich in quartz or carbonates (Formenti et al., 2014). Specific to Namibia, because of the strong
380 link between $nss-Ca^{2+}$ and fluorine, the $Fe/nss-Ca^{2+}$ ratio may also to distinguish dust influenced by
381 fluorspar mining.

382

Fig 5. *Scatterplot of Fe/nss-Ca^{2+} and Si/Al mass ratios for the samples collected at HBAO in period May-December 2017. Values obtained for samples collected during the dust events are represented as colored dots. Values for samples collected outside those events (background) are represented as grey dots.*

Figure 5 indicates that the range of variability of both Fe/nss-Ca^{2+} and Si/Al ratios is small when considering dust events only. The elemental ratios of samples collected during the background periods are rather similar to dust events during a same sampling period, except for Si/Al for the period between 19-26 May and for Fe/nss-Ca^{2+} for the samples of 18-25 September, when significant differences, not really explicable and not inducing a significant difference in the %SFe values are observed (**Fig. S3**).

The values for ambient dust measured at HBAO are consistent with those of the previous field observations in Namibia (Annegarn et al., 1983; Eltayeb et al., 1993), but also with values reported by Caponi et al. (2017) for laboratory-aerosolised dust from two soils collected on the Namibian gravel plains. This is in agreement of the indications of the emission maps (**Fig. 2**), showing significant emissions in the gravel plains. The absence of seasonal cycle in the elemental composition illustrated in **Fig. S3** suggests that the seasonal change from northern to southern sources does not induce a change in the composition of the aerosol dust sampled at HBAO, which is consistent with the fact that the northern and the southern gravel plains of Namibia have similar mineralogy (Heine and Vökel, 2010). This suggests that the mineralogical composition of mineral dust should not be a discriminating factor explaining the seasonality of the iron solubility observed at HBAO.

4.2.   Evidence of processing by marine biogenic emissions

The atmospheric (in-cloud) processing associated with secondary aerosol production may increase the fractional solubility of Fe during transport (Takahashi et al., 2011; Rodríguez et al., 2021). This has also been shown for Al and Ti (Baker et al., 2020). The chemical processing could include both acidic and ligand-promoted dissolution (Desboeufs et al., 2001, Longo et al., 2016, Tao et al., 2019). Oxalic acid has previously been used as a proxy for organic ligand–mediated iron dissolution pro-cesses because it is the most abundant species in the atmosphere and is the most effective ligand in promoting iron dissolution (Baker et al., 2020; Hamilton et al., 2021). However, several secondary compounds, such as carboxylate ligands and marine secondary products derived from dimethyl sul-fide (DMS) oxidation, have been identified as playing a role in increasing the soluble fraction of iron from mineral aerosols (Johansen and Key, 2006; Paris et al., 2011; Paris and Desboeufs, 2013; Woz-niak et al., 2013 and 2015). The increase of ligands-promoted dissolution is attributed to photochem-ical reduction of Fe(III) in Fe (II) (Siefert et al., 1994; Johansen and Key, 2006).

To investigate these aspects, the mass concentrations of the ionic compounds (oxalate, formate, MSA, NO_3^-, NH_4^+ and nss-SO_4^{2-}) implied in the secondary aerosol production, measured at HBAO during dust and background periods are reported in **Table 3.**

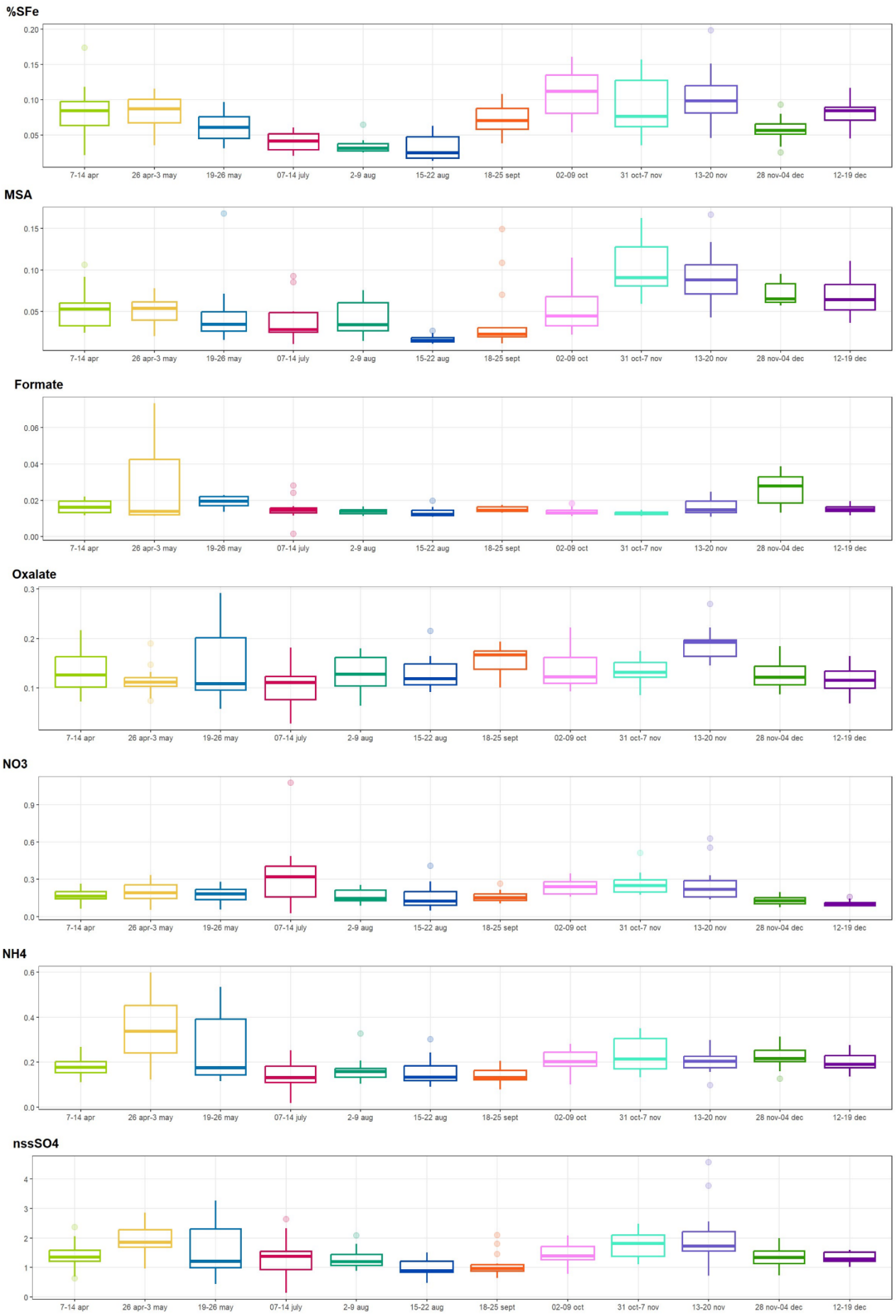*Table 3. Average and standard deviations of mass concentrations of water-soluble ions measured at HBAO during dust and background events from May to December 2017. Concentrations are expressed in ng m^{-3}. The number of samples pertaining to each occurrence is indicated in brackets.*

	Dust	**Background**
nss-SO_4^{2-}	1795 ± 762 (N = 42)	1366 ± 505 (N=132)
Oxalate	155 ± 53 (N = 42)	127 ± 35 (N = 132)
Formate	18 ± 6 (N = 40)	16 ± 9 (N = 105)
MSA	64 ± 37 (N=36)	56 ± 36 (N=114)
NO_3^-	205 ± 79 (N=42)	200 ± 138 (N=132)
NH_4^+	192 ± 71 (N=42)	207 ± 98 (N=132)

Oxalate was the most abundant organic compound, followed by MSA, a secondary product of DMS oxidation and a unique particulate tracer of the primary marine biogenic activity (Andreae et al., 1995). On average, organic compounds were equally concentrated in dust and background events. Amongst inorganic species, nss-SO_4^{2-} was the most concentrated compound, with higher values during the dust events than during the background period.
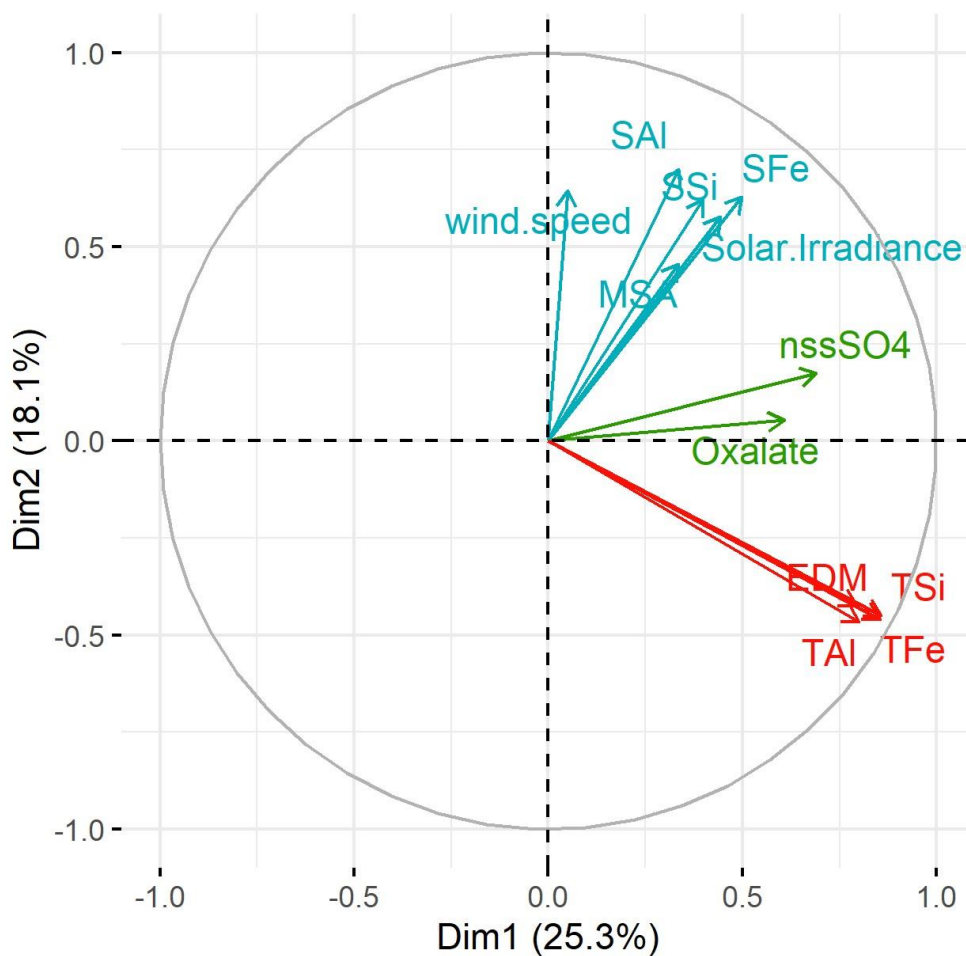
16

%SFe

MSA

Formate

Oxalate

NO3

NH4

nssSO4

431

432 **Fig. 6.** *Box-plots of the averages of %SFe and secondary organic and inorganic compounds mass concentrations (µg m^{-3})*
433 *for the sampling periods including all the samples (dust + background). Boxes and whiskers as in Fig. 2.*

434

435 Their detailed time series are shown in **Fig 6**, where it is compared to that of the iron fractional solu-

436 bility. There is no clear seasonal cycle for any of the ionic compounds, with the exception of MSA,

437 which shows a similar time variability than %SFe. MSA concentrations were lowest between May and

438 August (average 38.0 ± 28.0 ng m^{-3}), while higher concentrations were measured from September to

439 December (72.7 ± 38.1 ng m^{-3}). These differences are also observed for the dust cases only. The

440 average MSA concentration was 40.6 ± 23.4 ng m^{-3} for Dust 04 to Dust 08 episodes. It increased to

441 77.7 ± 35.3 ng m^{-3}, almost a factor of 2 between episodes Dust 09 and Dust 13. The mass concen-

442 trations and the seasonal cycle of MSA are related with the proximity of the strong coastal upwelling

443 by the Benguela current (Formenti et al., 2019; KL20). The maximum concentration of MSA (106.2

444 ng m^{-3}) was measured during episode Dust 11, which is also the time of the highest SFe% observa-

445 tion. This episode was also characterised by the highest oxalate, nss-SO_4^{2-} and NO_3^- concentrations.

446 However, no clear correlation between the %SFe and the secondary compounds concentrations can

447 be found in our data (**Fig. S4**). In order to statistically explore the potential links between %SFe and

448 various these concentrations, **Fig. 7** shows the correspondence plot between total Fe, Al and Si, and

449 their respective fractional solubility, the measured secondary compounds and the meteorological con-

450 ditions during sampling obtained from Principal Component Analysis (PCA) for all the samples. The

451 variables correlated in time are grouped together (the closer they are in the circle, the stronger the

452 correlation) whereas the variables which are anti-correlated are situated on the opposite side of the

453 plot origin.

454

The PCA plot (Fig.7) emphasizes 3 groups of dependent parameters: 1. a high correlation between total Fe, Al and Si concentrations and dust loading (EDM), as previously identified in Table 1 and Fig.3, 2. a relation between oxalate and nss-SO_4^{2-} concentrations, suggesting a common chemical process of formation, and 3.the dependence between %SFe (%SAl and %SSi), the MSA concentrations, the solar irradiance and to a lesser extent with the wind speed. While it is expected that the emission of mineral dust occurs when the wind speed is high, the correlation of %SFe with wind speed is rather surprising since the %SFe is independent of the dust load (Fig. 2 and 7). **Fig. S4** in the supplementary material present the plots between %SFe, MSA concentrations, solar irradiance and wind speed for background and dust events. The correlation between the wind speed and the MSA concentrations (Fig. S4) is consistent with Andreae et al. (1995), who demonstrated how, in this area due to persistent phytoplankton bloom, the atmospheric concentrations of dimethylsulphide (DMS),

the gaseous precursors of MSA, depend on the sea-to-air flux, in turn is determined by the concentrations in the ocean water and the surface wind speed..

As previously mentioned, Johansen and Key (2006) showed an increase of dissolution of ferrihydrite, a proxy of iron(oxy)hydroxide found in desert mineral dust, by photolysis of the Fe(III)-MSIA (methane sulfinic acid) complex, producing MSA and soluble Fe. Zhuang et al. (1992) proposed an increase of iron dissolution by the acidification of aerosol particles associated with dimethylsulphide (DMS) oxidation. Here, the link between the Fe fractional solubility, solar irradiance and MSA is in agreement with the photo-reduction dissolution of Fe by MSA condensation on Fe-bearing dust. Thus, we attribute the iron fractional solubility seasonality observed at HBAO both to solar irradiance and MSA temporal evolution via this process. It is interesting to note that due to the high correlation between %SFe and %SAl and %SSi, the photochemical processes could also impact the solubility of all element-bearing dust.

4.3. Link to other sources of iron and oxalate

Formenti et al. (2018) have shown that in the Austral winter, when the synoptic circulation is dominantly anti-cyclonic, air masses laden with light-absorbing aerosols either from ship pollution or biomass burning can be transported to HBAO (Formenti et al., 2018). However, the lowest Fe solubility (< 5%) was measured in July and August 2017, and no correlation between the %SFe and the percent mass fraction of iron from sources other than dust can be found in our data (not shown).

The mass apportionment of iron reported by KL20 indicates that, during the dust events and the background periods, respectively, 7% and 29% of the mass of total elemental Fe was not associated to mineral dust, but rather to a factor indicated as "ammonium-neutralised component", mostly characterised by secondary species, and non-sea-salt potassium (nss-K^+). The PMF analysis indicated that the "ammonium-neutralised component" was associated to photo-oxidation of marine biogenic emission but also episodically to biomass burning. This component includes oxalate, the most concentrated organic species at HBAO, and the strongest of the organic ligands promoting the photo-reduction of iron in mineral dust, henceforth the increase of its fractional solubility (Paris and Desboeufs, 2013). Surprisingly, excepted individual cases (Dust 13), our analysis does not show this strong link (Fig. 7), and indeed, contrary to the SFe%, the oxalate concentrations measured at HBAO was practically constant with time (in average 0.14+/- 0.04 µg.m^{-3}). The possible pathways of oxalate formation in this complex atmosphere are numerous through the year, from natural and anthropogenic sources (marine, heavy-oil combustion, biomass burning) and in-cloud and photo-oxidative processes (Baboukas et al., 2000; Myriokefalitakis et al., 2011).

5. Concluding remarks

For the first time, the fractional solubility of Fe in airborne atmospheric aerosols smaller than 10 µm in diameter is investigated along the west coast of Namibia, in southern Africa, a critical region for the global climate.

Ten intense episodes of transport of mineral dust from aeolian erosion were identified from the analysis of aerosol samples collected between May and December 2017 at the Henties Bay Aerosol Observatory (HBAO). Based on modelling and measurements, source regions were identified both in the northern and southern gravel plans. Our data do not provide any evidence of the possible contribution of dust from coastal riverbeds, which are considered to be frequent sources of atmospheric dust and soluble iron in the region (Vickery et al., 2013; Von Holdt et al., 2017; Dansie et al., 2017a; 2017b). The total iron represents, on average, 5.8 % (± 0.6 %) of the total dust mass, and that the average water-soluble Fe fractional solubility is 6.9 % (± 3.3 %). These values should be useful to atmospheric models estimating the dust-borne input of soluble Fe from the gravel plains in Namibia to the surrounding oceans.

The seasonal increase of the iron fractional solubility is associated to that of the concentrations of MSA and correlated to meteorological parameters such as the wind speed and the surface solar irradiance. Our observations support the role of photo-chemical processes in the dissolution of Fe in our samples, and suggest that the oxidation of the marine biogenic emissions from the northern Benguela upwelling, favoured under high wind speed conditions, could play a significant role in increasing the solubility of elemental iron in mineral dust aerosols over coastal Namibia. This is in agreement with the mechanism described by Zhuang et al. (1992), who proposed an increase of iron dissolution by the acidification of aerosol particles associated with DMS oxidation, and Johansen and Key (2006), who showed an increase of dissolution of ferrihydrite, a proxy of iron(oxy)hydroxide found in desert mineral dust, by photolysis of the Fe(III)-MSIA (methane sulfinic acid) complex, producing MSA and soluble Fe. It is interesting to note that due to the high correlation between %SFe and %SAl and %SSi (and %STi), the same photochemical processes could also impact the solubility of all element-bearing dust. The possible mechanism suggested by this paper could be responsible for initiating a feedback loop whereby the input of dust of increased trace and major elements solubility would result in stronger marine biogenic emissions to the atmosphere. This possible mechanism could increase the iron solubility in mineral dust, maybe also initiating a feedback loop whereby the input of dust of increased solubility would result in stronger marine biogenic emissions to the atmosphere, including Volatile Organic Compounds (VOCs), in particular butene, massively emitted by the organisms in the coastal marine foam (Giorio et al., 2022).This complex and dynamic environment where the interplay between the input of atmospheric iron from transported dust and the marine biogenic emissions from the Benguela oceanic upwelling system should be further addressed by future research.

Author contributions. PF, DK, SJP, AN, MC, AF and SC prepared and performed the filter sampling. RT, KD, PF, SC, ST,and CMB performed the XRF, IC and ICP analysis of the collected samples. BL performed the field implementation. KS and SF performed the model calculations of dust emission fluxes. JPC performed the model calculations of air mass back-trajectories. HA and JC provided with the satellite retrieval of fog and low clouds. PF, KD, RT and SJP analysed and interpreted the dataset. PF and KD wrote the paper with contributions from RT and SJP, and the remaining authors. PF and SJP provided funding. PF coordinated the research activity and supervised its planning and execution.

Competing interests. PF is guest editor for the ACP Special Issue "New observations and related modelling studies of the aerosol–cloud–climate system in the Southeast Atlantic and southern Africa regions". The remaining authors declare that they have no conflicts of interests.

Special issue statement. This article is part of the special issue "New observations and related modelling studies of the aerosol–cloud–climate system in the Southeast Atlantic and southern Africa regions (ACP/AMT inter-journal SI)". It is not associated with a conference.

References

Andersen, H. and Cermak, J.: First fully diurnal fog and low cloud satellite detection reveals life cycle in the Namib, Atmos. Meas. Tech., 11, 5461–5470, doi: 10.5194/amt-11-5461-2018, 2018.

Andersen, H., Cermak, J., Solodovnik, I., Lelli, L. and Vogt, R.: Spatiotemporal dynamics of fog and low clouds in the Namib unveiled with ground- and space-based observations, Atmos. Chem. Phys., 1, 4383–4392, doi: 10.5194/acp-19-4383-2019, 2019.

Andersen, H., Cermak, J., Fuchs, J., Knippertz, P., Gaetani, M., Quinting, J., Sippel, S., and Vogt, R.: Synoptic-scale controls of fog and low-cloud variability in the Namib Desert, Atmos. Chem. Phys., 20, 3415–3438, https://doi.org/10.5194/acp-20-3415-2020, 2020.

Andreae, M. O.: Soot Carbon and Excess Fine Potassium: Long-Range Transport of Combustion-Derived Aerosols, Science, 220, 1148-1151, doi:10.1126/science.220.4602.1148, 1983.

Andreae, M. O., Elbert, W., and de Mora, S. J.: Biogenic sulfur emissions and aerosols over the tropical South Atlantic: 3. Atmospheric dimethylsulfide, aerosols and cloud condensation nuclei, J. Geophys. Res., 100, 11335-11356, https://doi.org/10.1029/94JD02828, 1995.

Annegarn, H.J., van Grieken, R.E., Bibby, D.M. and von Blottnitz, F.: Background Aerosol Composition in the Namib Desert, South West Africa (Namibia), Atmos. Environ., 17, 2045–2053, doi: 10.1016/0004-6981(83)90361-X, 1983.

Bhattachan, A., D'Odorico, P., Baddock, M.C., Zobeck, T.M., Okin, G.S., Cassar, N.: The Southern Kalahari: a potential new dust source in the Southern hemisphere?, Environ. Res. Lett., 7, 024001. http://dx.doi.org/10.1088/1748-9326/7/2/024001, 2012.

Bhattachan, A., P. D'Odorico, and G. S. Okin, Biogeochemistry of dust sources in Southern Africa, J. Arid Environ., 117, 18-27, http://dx.doi.org/10.1016/j.jaridenv.2015.02.013, 2015.

Baboukas, E. D., Kanakidou, M., and Mihalopoulos, N.: Carboxylic acids in gas and particulate phase above the Atlantic Ocean, J. Geophys. Res., 105, 14459–14471, https://doi.org/10.1029/1999JD900977, 2000.

Baker A.R., T. D. Jickells, M. Witt, and K. L. Linge, Trends in the solubility of iron, aluminium, manganese and phosphorus in aerosol collected over the Atlantic Ocean., Marine Chem., 98, 43-58, https://doi.org/10.1016/j.marchem.2005.06.004, 2006.

Baker, A. R., and T. D. Jickells, Mineral particle size as a control on aerosol iron solubility, Geophys. Res. Lett., 33, L17608. https://doi.org/10.1029/2006GL026557, 2006.

Baker, A. R., C. Adams C., T. G. Bell, T. D. Jickells, and L. Ganzeveld, Estimation of atmospheric nutrient inputs to the Atlantic Ocean from 50°N to 50°S based on large-scale field sampling: iron and other dust-associated elements, Glob. Biogeochem. Cycles, 27, 755–767, doi:10.1002/gbc.20062, 2013.

Baker, A. R., M. Thomas, H. W. Bange, and E. Plasencia Sánchez, E., Soluble trace metals in aerosols over the tropical south-east Pacific offshore of Peru, Biogeosciences, 13, 817–825, https://doi.org/10.5194/bg-13-817-2016, 2016.

615   Baker, Alex R., et T. D. Jickells, Atmospheric deposition of soluble trace elements along the Atlantic Meridional
616   Transect (AMT), in *The Atlantic Meridional Transect programme (1995-2016)* 158: 41-51.
617   https://doi.org/10.1016/j.pocean.2016.10.002, 2017.

618   Baker, A. R., M. Li, and R. Chance, Trace metal fractional solubility in size-segregated aerosols from the tropical
619   eastern Atlantic Ocean, Global Biogeochemical Cycles, 34, e2019GB006510.
620   https://doi.org/10.1029/2019GB006510, 2020.

621   Bryant, R. G., Bigg, G. R., Mahowald, N. M., Eckardt, F. D., and Ross, S. G., Dust emission response to climate
622   in southern Africa, J. Geophys. Res., 112, D09207, doi:10.1029/2005JD007025, 2007.

623   Caponi, L., Formenti, P., Massabó, D., Di Biagio, C., Cazaunau, M., Pangui, E., Chevaillier, S., Landrot, G.,
624   Andreae, M. O., Kandler, K., Piketh, S., Saeed, T., Seibert, D., Williams, E., Balkanski, Y., Prati, P., and
625   Doussin, J.-F.: Spectral- and size-resolved mass absorption efficiency of mineral dust aerosols in the
626   shortwave spectrum: a simulation chamber study, Atmos. Chem. Phys., 17, 7175–7191,
627   https://doi.org/10.5194/acp-17-7175-2017, 2017.

628   Chaboureau, J.-P., L. Labbouz, C. Flamant, and A. Hodzic. Acceleration of the southern African easterly jet
629   driven by radiative effect of biomass burning aerosols and its impact on transport during AEROCLO-sA, At-
630   mos. Chem. Phys.,22, 8639-8658, https://doi.org/10.5194/acp-22-8639-2022, 2022.

631   Chance R, T. D. Jickells and A. R. Baker, Atmospheric trace metal concentrations, solubility and deposition
632   fluxes in remote marine air over the south-east Atlantic, Marine Chemistry, 177, 45–56, doi:10.1016/j.mar-
633   chem.2015.06.028, 2015.

634   Dansie, A. P., G. F. S. Wiggs, D. S. G. Thomas, and R. Washington, Measurements of windblown dust charac-
635   teristics and ocean fertilisation potential: The ephemeral river valleys of Namibia, Aeolian Res., 29, 30–41,
636   doi:10.1016/j.aeolia.2017.08.002, 2017a.

637   Dansie, A. P., G. F. S. Wiggs, and D. S. G. Thomas, Iron and nutrient content of wind-erodible sediment in the
638   ephemeral river valleys of Namibia, Geomorphology, 290, 335-346, https://doi.org/10.1016/j.geo-
639   morph.2017.03.016, 2017b.

640   Dansie AP, Thomas DSG, Wiggs GFS, Baddock MC, Ashpole I. Plumes and blooms - Locally-sourced Fe-rich
641   aeolian mineral dust drives phytoplankton growth off southwest Africa. Sci Total Environ., doi: 10.1016/j.sci-
642   totenv.2022.154562, 2022.

643   Desboeufs, K. V., R. Losno, et J. L. Colin, Factors influencing aerosol solubility during cloud processes, Atmos.
644   Environ., 35, 3529-3537, https://doi.org/10.1016/S1352-2310(00)00472-6, 2001.

645   Desboeufs, K.V., Sofikitis, A., Losno, R., Colin, J.L., Ausset, P. Dissolution and solubility of trace metals from
646   natural and anthropogenic aerosol particulate matter, Chemosphere 58, 195–203, 2005.

647   Desboeufs, K., Fu, Y., Bressac, M., Tovar-Sánchez, A., Triquet, S., Doussin, J.F., Giorio, C., Chazette, P.,
648   Disnaquet, J., Feron, A., Formenti, P., Maisonneuve, F., Rodríguez-Romero, A., Zapf, P., Dulac, F., and
649   Guieu, C., Wet deposition in the remote western and central Mediterranean as a source of trace metals to
650   surface seawater, Atmos. Chem. Phys., 22, 2309–2332, https://doi.org/10.5194/acp-22-2309-2022, 2022.

651 Eltayeb, M.A.; Van Grieken, R.E., Maenhaut, W. and Annegarn, H.J.: Aerosol-Soil Fractionation for Namib De-
652   sert Samples. Atmos. Environ., 27(5), https://doi.org/10.1016/0960-1686(93)90185-2, 1993.

653 Feuerstein, S., and Schepanski, K.: Identification of Dust Sources in a Saharan Dust Hot-Spot and Their Imple-
654   mentation in a Dust-Emission Model, Remote Sensing, 11, doi:10.3390/rs110100004, 2019.

655 Flamant, C., M. Gaetani, J.-P. Chaboureau, P. Chazette, S. J. Piketh, and P. Formenti. Smoke in the river: an
656   Aerosols, Radiation and Clouds in southern Africa (AEROCLO-sA) case study, Atmos. Chem. Phys., 22,
657   5701–5724, https://doi.org/10.5194/acp-22-5701-2022, 2022.

658 Formenti, P., Schütz, L., Balkanski, Y., Desboeufs, K., Ebert, M., Kandler, K., Petzold, A., Scheuvens, D.,
659   Weinbruch, S., and Zhang, D.: Recent progress in understanding physical and chemical properties of African
660   and Asian mineral dust, Atmos. Chem. Phys., 11, 8231–8256, https://doi.org/10.5194/acp-11-8231-2011,
661   2011.

662 Formenti, P., S. Caquineau, K. Desboeufs, A. Klaver, S. Chevaillier, E. Journet, J. L. Rajot, Mapping the phys-
663   ico-chemical properties of mineral dust in western Africa: mineralogical composition, Atmos. Chem. Phys., 14,
664   10663-1068, 2014.

665 Formenti, P., Piketh, S. J., Namwoonde, A., Klopper, D., Burger, R., Cazaunau, M., Feron, A., Gaimoz, C.,
666   Broccardo, S., Walton, N., Desboeufs, K., Siour, G., Hanghome, M., Mafwila, S., Omoregie, E., Junkermann,
667   W., and Maenhaut, W.: Three years of measurements of light-absorbing aerosols over coastal Namibia: sea-
668   sonality, origin, and transport, Atmos. Chem. Phys., 18, 17003-17016, https://doi.org/10.5194/acp-18-17003-
669   2018, 2018.

670 Formenti, P., B. D'Anna, C. Flamant, M. Mallet, S.J. Piketh, K. Schepanski, F. Waquet, F. Auriol, G. Brogniez,
671   F. Burnet, J. Chaboureau, A. Chauvigné, P. Chazette, C. Denjean, K. Desboeufs, J. Doussin, N. Elguindi, S.
672   Feuerstein, M. Gaetani, C. Giorio, D. Klopper, M.D. Mallet, P. Nabat, A. Monod, F. Solmon, A. Namwoonde,
673   C. Chikwililwa, R. Mushi, E.J. Welton, and B. Holben, The Aerosols, Radiation and Clouds in Southern Africa
674   Field Campaign in Namibia: Overview, Illustrative Observations, and Way Forward, Bull. Amer. Meteor. Soc.,
675   100, 1277–1298, https://doi.org/10.1175/BAMS-D-17-0278.1, 2019.

676 Gao, Y., Xu, G., Zhan, J., Zhang, J., Li, W., Lin, Q., Chen, L., and Lin, H., Spatial and particle size distributions
677   of atmospheric dissolvable iron in aerosols and its input to the Southern Ocean and coastal East Antarctica,
678   J. Geophys. Res., 118, 12,634–12,648, doi:10.1002/2013JD020367, 2013.

679 Gili, S., Vanderstraeten, A., Chaput, A., King, J., Gaiero, D. M., Delmonte, B., Vallelonga, Paola Formenti,
680   Claudia Di-Biagio, Mathieu Cazaunau, Edouard Pangui, Jean-Francois Doussin, Mattielli, N., South African
681   dust contribution to the high southern latitudes and East Antarctica during interglacial stages, Communications
682   Earth & Environment, 3, 129, https://doi.org/10.1038/s43247-022-00464-z, 2022.

683 Ginoux, P., Prospero, J.M., Gill, T.E., Hsu, N.C., Zhao, M.: Global-scale attribution of anthropogenic and natural
684   dust sources and their emission rates based on MODIS Deep Blue aerosols products, Rev. Geophys., 50,
685   RG3005, doi:10.1029/2012RG000388, 2012.

686 Giorio, C., Doussin, J.F., D'Anna, B., Mas, S., Filippi, D., Denjean, C., Mallet,M.D., Bourrianne,T., Burnet, F,
687   Cazanaur,M., Chikwililwa, C., Desboeufs, K., Feron, A., Michoud, V., Namwoonde, A., Andreae, M.O., Piketh,

S.J. and Formenti, P.: Butene emissions from coastal ecosystems may contribute to new particle formation, Geophys. Res. Lett., 49, https://doi.org/10.1029/2022GL098770, 2022.

Grini, A., Tulet, P., and Gomes, L.: Dusty weather forecasts using the MesoNH mesoscale atmospheric model. J. Geophys. Res., 111, D19205, https://doi.org/10.1029/2005JD007007, 2006.

Hamilton, D. S., Perron, M.M.G., Bond, T.C., Bowie, A.R., Buchholz, R.R., Guieu, C., Ito, A., Maenhaut, W., Myriokefalitakis, S., Olgun, N., Rathod, S.D., Schepanski, K., Tagliabue, A., Wagner, R. and Mahowald, N.M.: Earth, wind, fire, and pollution: Aerosol nutrient sources and impacts on ocean biogeochemistry, Annual review of Marine Science, 14, pp. 303- 330, https://doi.org/10.1146/annurev-marine-031921-013612, 2021.

Heike, K and J. Volkel, Soil clay minerals in Namibia and their significance for the terrestrial and marine past global change, African Study Monographs, Suppl.40, 2010.

Heimburger, A., Losno, R., and Triquet, S.: Solubility of iron and other trace elements in rainwater collected on the Kerguelen Islands (South Indian Ocean), Biogeosciences, 10, 6617–6628, https://doi.org/10.5194/bg-10-6617-2013, 2013.

Hooper, H., Mayewski, P., Marx, S., Henson, S., Potocki, M., Sneed, S., Handley, M., Gasso, S., Fischer, M., Saunders, K.M., Examining links between dust deposition and phytoplankton response using ice cores. Aeolian Res., 36, 45-60, https://doi.org/10.1016/j.aeolia.2018.11.001, 2019.

Ito, A., and Kok, J. F.: Do dust emissions from sparsely vegetated regions dominate atmospheric iron supply to the Southern Ocean?, J. Geophys. Res., 122, 3987-4002, https://doi.org/10.1002/2016JD025939, 2017.

Ito, A., Y. Ye, C. Baldo, and Z. Shi, Ocean Fertilization by Pyrogenic Aerosol Iron. npj Climate Atmos. Sci., 4, 30, doi: 10.1038/s41612-021-00185-8, 2021.

Jickells, T., Andersen, K.K., Baker, A., Bergametti, G., Brooks, N., Cao, J., Boyd, P., Duce, R., Hunter, K., Global iron connections between desert dust, ocean biogeochemistry, and climate, Science, 308, 67-71, DOI: 10.1126/science.1105959, 2005.

Journet, E., Desboeufs, K., Caquineau, S. and Colin, J. L.: Mineralogy as a critical factor of dust iron solublity, Geophys. Res. Lett., 35, https://doi.org/10.1029/2007GL031589, 2008.

Johansen, A. M., and Key, J. M.: Photoreductive dissolution of ferrihydrite by methanesulfinic acid: Evidence of a direct link between dimethylsulfide and iron-bioavailability, Geophys. Res. Lett., 33, L14818, doi:10.1029/2006GL026010, 2006.

Kaplan, J.O., Bigelow, N.H., Prentice, I.C., Harrison, S.P., Bartlein, P.J., Christensen, T.R., Cramer, W., Matveyeva, N.V., McGuire, A.D., Murray, D.F., Razzhivin, V.Y., Smith, B., Walker, D.A., Anderson, P.M., Andreev, A.A., Brubaker, L.B., Edwards, M.E. and Lozhkin A.V.: Climate change and Arctic ecosystems: 2. Modeling, paleodata-model comparison and future projections, J. Atmos. Res., 108, 8171, doi: 10.1029/2002JD002559, 2003.

Kangueehi, K. I., Southern African dust characteristics and potential impacts on the surrounding oceans, PhD Thesis, Stellenbosch University, http://hdl.handle.net/10019.1/123923, 2021.

723 Klopper, D., Formenti, P., Namwoonde, A., Cazaunau, M., Chevaillier, S., Feron, A., Gaimoz, C., Hease, P.,
724   Lahmidi, F., Mirande-Bret, C., Triquet, S., Zeng, Z. And Piketh, S.J.: Chemical composition and source appor-
725   tionment of atmospheric aerosols on the Namibian Coast, Atmos. Chem. Phys., 20, pp. 15811 – 15833,
726   https://doi.org/10.5194/acp-20-15811-2020, 2020.

727 Kok, J. F., Albani, S., Mahowald, N. M., and Ward, D. S.: An improved dust emission model – Part 2: Evaluation
728   in the Community Earth System Model, with implications for the use of dust source functions, Atmos. Chem.
729   Phys., 14, 13043–13061, https://doi.org/10.5194/acp-14-13043-2014, 2014.

730 Kok, J.F., Ridley, D.A., Zhou, Q., Miller, R.L., Zhao, C., Heald, C.L., Ward, D.S., Albani, S., Haustein, K.: Smaller
731   desert dust cooling effect estimated from analysis of dust size and abundance. Nature Geoscience, 10, 274–
732   278, https://doi.org/10.1038/ngeo2912, 2017.

733 Laurent, B., Marticorena, B., Bergametti, G., Chazette, P., Maignan, F. and Schmechtig C.: Simulation of the
734   mineral dust emission frequencies from desert areas of China and Mongolia using an aerodynamic roughness
735   length map derived from POLDER/ADEOS 1 surface products, J. Geophys. Res., 110, D18, doi:
736   10.1029/2004JD005013, 2005.

737 Lide, D. R.: CRC Handbook of Chemistry and Physics 1991–1992, CRC Press, Boca Raton, Florida, 1992.

738 Liu, M., Matsui, H., Hamilton, D.S., Lamb, K.D., Rathod, S.D., Schwarz, J.P. and Mahowald, N.M.: The underap-
739   preciated role of anthropogenic sources in atmospheric soluble iron flux to the Southern Ocean, Climate At-
740   mos. Sci., 5, 28, https://doi.org/10.1038/s41612-022-00250-w, 2022.

741 Longo, A., F. Y. Feng, B., W. M. Landing, R.U. Shelley, A. Nenes, N. Mihalopoulos, K. Violaki, E. D. Ingall.
742   Influence of Atmospheric Processes on the Solubility and Composition of Iron in Saharan Dust, Environ. Sci.
743   Tech., 50, 13: 6912-20. https://doi.org/10.1021/acs.est.6b02605, 2016.

744 Mahowald, N., Luo, C., del Corral, J., Zender, C.S.: Interannual variablity in atmospheric mineral aerosols from
745   a 22-year model simulation and observational data, J. Geophys. Res., 108 (D12),
746   https://doi.org/10.1029/2002JD002821, 2003.

747 Marcotte, A.R., Anbar, A.D., Majestic, B.J., Herckes, P.: Mineral dust and iron solubility: Effects of composition,
748   particle size, and surface area, Atmosphere, 11, 533, doi:10.3390/atmos11050533, 2020.

749 Marticorena, B. and Bergametti, G.: Modelling the atmospheric dust cycle: 1. Design of a soil-derived dust
750   emission scheme, J. Geochem. Res., 16415-16430, 1995.

751 Marticorena, B., Chazette, P., Bergametti, G., Dulac, F., Legrand, M.: Mapping the aerodynamic roughness
752   length of desert surfaces from the POLDER/ADEOS bi-directional reflectance product, Int. J. Remote Sens.,
753   25, 603– 626, 2004.

754 Myriokefalitakis, S., Tsigarid is, K., Mihalopoulos, N., Scia re, J., Nenes, A., Kawamura,K., Segers, A., and
755   Kanakidou, M.: In-cloud oxalate formation in the global troposphere: a 3-D modeling study, Atmos. Chem.
756   Phys., 11, 5761-5782, doi:10.5194/acp-11-5761-2011, 2011.

757 Paris, R., Desboeufs, K. V., Formenti, P., Nava, S., and Chou, C.: Chemical characterisation of iron in dust and
758   biomass burning aerosols during AMMA-SOP0/DABEX: implication for iron solubility, Atmos. Chem. Phys.,
759   10, 4273–4282, https://doi.org/10.5194/acp-10-4273-2010, 2010.

760 Paris, R., K.V. Desboeufs, et E. Journet. Variability of dust iron solubility in atmospheric waters: Investigation of
761   the role of oxalate organic complexation, Atmos. Environ., 45, 6510-17. https://doi.org/10.1016/j.at-
762   mosenv.2011.08.068, 2011.

763 Paris, R., and K. V. Desboeufs, Effect of atmospheric organic complexation on iron-bearing dust solubility. At-
764   mos. Chem. Phys., 13, 4895-4905, https://doi.org/10.5194/acp-13-4895-2013, 2013.

765 Perron, M. M. G., Strzelec, M., Gault-Ringold, M., Proemse, B. C., Boyd, P. W., and Bowie, A. R.: Assessment
766   of leaching protocols to determine the solubility of trace metals in aerosols, Talanta, 208, 120377,
767   https://doi.org/10.1016/j.talanta.2019.120377, 2020.

768 Prospero, J.M., Ginoux, P., Torres, O., Nicholson S.E. and Gill, T.M.: Environmental characterization of global
769   sources of atmospheric soil dust identified with the Nimbus 7 total ozone mapping spectrometer (TOMS) ab-
770   sorbing aerosol product. Reviews of Geophysics, 40 (1): 1002, https://doi.org/10.1029/2000RG000095, 2002.

771 Redemann, J., Wood, R., Zuidema, P., Doherty, S. J., Luna, B., LeBlanc, S. E., Diamond, M. S., Shinozuka, Y.,
772   Chang, I. Y., Ueyama, R., Pfister, L., Ryoo, J.-M., Dobracki, A. N., da Silva, A. M., Longo, K. M., Kacenelen-
773   bogen, M. S., Flynn, C. J., Pistone, K., Knox, N. M., Piketh, S. J., Haywood, J. M., Formenti, P., Mallet, M.,
774   Stier, P., Ackerman, A. S., Bauer, S. E., Fridlind, A. M., Carmichael, G. R., Saide, P. E., Ferrada, G. A., Howell,
775   S. G., Freitag, S., Cairns, B., Holben, B. N., Knobelspiesse, K. D., Tanelli, S., L'Ecuyer, T. S., Dzambo, A. M.,
776   Sy, O. O., McFarquhar, G. M., Poellot, M. R., Gupta, S., O'Brien, J. R., Nenes, A., Kacarab, M., Wong, J. P.
777   S., Small-Griswold, J. D., Thornhill, K. L., Noone, D., Podolske, J. R., Schmidt, K. S., Pilewskie, P., Chen, H.,
778   Cochrane, S. P., Sedlacek, A. J., Lang, T. J., Stith, E., Segal-Rozenhaimer, M., Ferrare, R. A., Burton, S. P.,
779   Hostetler, C. A., Diner, D. J., Seidel, F. C., Platnick, S. E., Myers, J. S., Meyer, K. G., Spangenberg, D. A.,
780   Maring, H., and Gao, L.: An overview of the ORACLES (ObseRvations of Aerosols above CLouds and their
781   intEractionS) project: aerosol–cloud–radiation interactions in the southeast Atlantic basin, Atmos. Chem.
782   Phys., 21, 1507–1563, https://doi.org/10.5194/acp-21-1507-2021, 2021.

783 Reichholf, J. H., Is Saharan Dust a Major Source of Nutrients for the Amazonian Rain Forest?, Studies on
784   Neotropical Fauna and Environment, 21:4, 251-255, DOI: 10.1080/01650528609360710, 1986.

785 Rodríguez, S., Prospero, J.M., Lopez-Darias, J., Garcia-Alvarez, M.I., Zuidema, P., Nava, S., Lucarelli, F., Gas-
786   ton, C.J., Galindo, L., Sosa, E.: Tracking the changes of iron solubility and air pollutants traces as African dust
787   transits the Atlantic in the Saharan dust outbreaks. Atmos. Environ., 246, 118092, https://doi.org/10.1016/j.at-
788   mosenv.2020.118092, 2021.

789 Rodríguez, S., Riera, R., Fonteneau, A., Alonso-Pérez, S., and López-Darias, J.: African desert dust influences
790   migrations and fisheries of the Atlantic skipjack-tuna, Atmospheric Environment, 312, 120022,
791   https://doi.org/10.1016/j.atmosenv.2023.120022, 2023.

792 Shelley, R.U., Morton, P.L., Landing, W.M., Elemental ratios and enrichment factors in aerosols from the US-
793   GEOTRACES North Atlantic transects. Deep-Sea Res. II, 2014.

794 Shelley, R. U., Landing, W. M., Ussher, S. J., Planquette, H., & Sarthou, G. Regional trends in the fractional
795   solubility of Fe and other metals from North Atlantic aerosols (GEOTRACES cruises GA01 and GA03) follow-
796   ing a two-stage leach, Biogeosciences, 15(8), 2271–2288. https://doi.org/10.5194/bg-15-2271-2018, 2018.

797 Sholkovitz, E.R., Sedwick, P.N., Church, T.M. Influence of anthropogenic combustion emissions on the deposi-
798   tion of soluble aerosol iron to the ocean: empirical estimates for island sites in the North Atlantic, Geochim.
799   Cosmochim. Acta, 73, 3981–4003, http://dx.doi.org/10.1016/j.gca.2009.04.029, 2009.

800 Siefert, R. L., S. O. Pehkonen, Y. Erel, and M. R. Hoffman, Iron photochemistry of aqueous suspensions of
801   ambient aerosol with added organic acids, Geochim. Cosmochim. Acta, 58, 3271–3279, 1994.

802 Spirig, R., Vogt, R., Larsen, J. A., Feigenwinter, C., Wicki, A., Franceschi, J., Parlow, E., Adler, B., Kalthoff, N.,
803   Cermak, J., Andersen, H., Fuchs, J., Bott, A., Hacker, M., Wagner, N., Maggs-Kölling, G., Wassenaar, T. and
804   Seely, M.: Probing the fog life-cycles in the Namib desert, Bull. Am. Met. Soc., 100, 2491-2508,
805   doi:10.1175/bams-d-18-0142.1, 2019.

806 Swan, H.B., and J. P. Ivey, Elevated particulate methanesulfonate, oxalate and iron over Sydney Harbour in the
807   austral summer of 2019-20 during unprecedent bushfire activity, Atmos. Environ., 226, 118739,
808   https://doi.org/10.1016/j.atmosenv.2021.118739, 2021.

809 Swap, R., Garstang, M., Macko, S.A., et al., The long–range transport of southern African aerosols to the tropical
810   South Atlantic. J. Geophys. Res., 101, 23777–23791, https://doi.org/10.1029/95jd01049, 1996.

811 Takahashi, Y., Higashi, M., Fukurawa, T., Mitsunobu, S.: Change of iron species and iron solubility in Asian
812   dust during the long-range transport from western China to Japan, Atmos. Chem. Phys, 11, 11237-11252,
813   doi:10.5194/acp-11-11237-2011, 2011.

814 Tao, Y., Murphy, J.G.: The mechanisms responsible for the interactions among oxalate, pH, and Fe dissolution
815   in $PM_{2.5}$. Earth and Space Chemistry, 3, 2259-2265, https://doi.org/10.1021/acsearthspacechem.9b00172,
816   2019.

817 Tegen, I., Schepanski, K.: The Global distribution of Mineral Dust, IOP Conference Series: Earth and Environ-
818   mental Sciences, 7, 012001, doi:10.1088/1755-1307/7/1/012001, 2009.

819 Tyson, P. D. and Preston-Whyte, R. A.: The Weather and Climate of Southern Africa, 2nd ed., Oxford University
820   Press Southern Africa, Cape Town, 2014.

821 Ventura, A., Simões, E.F.C., Almeida, A.S., Martins, R., Duarte, A.C., Loureiro, S., Duarte, R.M.B.O., Deposition
822   of aerosols onto upper ocean and their impacts on marine biota, Atmosphere, 12, 684,
823   https://doi.org/10.3390/atmos12060684, 2021.

824 Vickery, K.J., Eckardt, F.D.: Dust emission controls on the lower Kuiseb River valley, Central Namib, Aeolian
825   Res., 10, 125-133, https://doi.org/10.1016/j.aeolia.2013.02.006, 2013.

826 von Holdt, J.R., Eckardt, F.D., Wiggs, G.F.S.: Landsat identifies aeolian dust emission dynamics at the landform
827   scale, Remote Sensing Environ., 198, 229-243, https://doi.org/10.1016/j.rse.2017.06.010, 2017.

828 Wozniak, A. S.; Shelley, R. U.; Sleighter, R. L.; Abdulla, H. A. N.; Morton, P. L.; Landing, W. M.; Hatcher, P. G.
829   Relationships among aerosol water soluble organic matter, iron and aluminium in European, North African,

830   and Marine air masses from the 2010 US GEOTRACES cruise, Mar. Chem., 154, 24– 33 DOI: 10.1016/j.mar-
831   chem.2013.04.011, 2013.

832   Wozniak, A. S., R.U. Shelley, S.D. McElhenie, W.M. Landing, P. G. Hatcher. Aerosol water soluble organic
833   matter characteristics over the North Atlantic Ocean: Implications for iron-binding ligands and iron solubility.
834   SCOR WG 139: Organic Ligands – A Key Control on Trace Metal Biogeochemistry in the Ocean 173: 162-72.
835   https://doi.org/10.1016/j.marchem.2014.11.002, 2015.

836   Zhuang, G., Z. Yi, R. A. Duce, and Brown, P.R.: Link between iron and sulphur cycles suggested by detection
837   of Fe (II) in remote marine aerosols, Nature, 355, pp. 537–539, https://doi.org/10.1038/355537a0, 1992.

838

839